Romanian Reports in Physics, Vol. 62, No. 3, P. 429–443, 2010

LASERS AND LASER SYSTEMS

Dedicated to the 50th LASER Anniversary
(LASERFEST-50)

SENSITIZATION OF Yb^{3+} EMISSION IN LASER OXIDE CERAMICS

V. LUPEI[1], A. LUPEI[1], A. IKESUE[2], C. GHEORGHE[1], S. HAU[1]

[1]*National Institute of Lasers, Plasma and Radiation Physics, Magurele-Bucharest, R-077125, Romania, E-mail: lupei_voicu@yahoo.com*
[2]*World-Lab. Co. Ltd., Atsuta-ku, Nagoya 456-8587, Japan*

(Received May 31, 2010)

Abstract. The co-doping of the laser materials to create the possibilities of exitation with visible strong pulsed pump sources (flash lamps) of i.r. Yb^{3+} emission were explored. Two new options for the sensitization of Yb^{3+} emission in laser oxide ceramics (by Nd^{3+} in YAG and Cr^{3+} in Sc_2O_3) were spectroscopically investigated. The characteristics of the Nd→Yb energy transfer in (Nd, Yb) co-doped YAG were compared to those in Y_2O_3 ceramics, in connection with specific spectroscopic properties and structures. The good overlap of $^4T_2 \rightarrow {}^4A_2$ broad emission of C_{3i} Cr^{3+} center in Sc_2O_3 with Yb^{3+} absorption determine an efficient resonant energy transfer from Cr^{3+} to Yb^{3+} in (Cr, Yb): Sc_2O_3 co-doped ceramics; the mechanisms and energy transfer parameters were evaluated.

Key words: sensitized emission of Yb, transparent ceramic, (Nd,Yb): YAG, (Cr, Yb): Sc_2O_3.

1. INTRODUCTION

Owing to its electronic structure, with only two energy manifolds, which prevents parasitic de-excitation by cross-relaxation, energy transfer up-conversion or excited state absorption, Yb^{3+} ion has very attractive characteristics for laser emission in the ~ 1 micron range. The Yb^{3+} lasers operate in quasi-three-level scheme, with low quantum defect and reduced heat generation. The long lifetime of Yb^{3+} metastable level favors low threshold in continuous-wave and high storage for Q-switch operation, whereas the broad emission lines show prospect for tunable or ultra-short pulse generation. In most laser materials the absorption cross-section of Yb^{3+} is quite small. Long laser active components such as fibers, or multipass of the pumping radiation, as in the thin disk lasers can be used to grant efficient absorption of pump radiation and diode pumped industrial class lasers based on

these approaches exist. However, the applications based on bulk laser materials such as high-energy laser emission would, however, require high doping concentrations, which could favor increased laser reabsorption, energy migration to accidental impurities, up conversion by cooperative processes, as well as reduction of the thermal conductivity of the material.

A major drawback of Yb^{3+} ions is the lack of absorption bands in visible, the region where strong pulsed pump sources (flash lamps) exist, making impossible exploitation of the good storage capacity for generation of very high energy Q-switched laser emission. A solution to overcome this difficulty could be co-doping of the laser material with ions (sensitizers – *donors*) able to absorb efficiently the radiation of these pump sources and to transfer the excitation to the Yb^{3+} ions – *acceptors*, with the condition that the energy transfer from the donor to acceptors to be very efficient. As sensitizers one could use transition metal ions (most studies refers to Cr^{3+} ions) or other rare earth ions [1, 2].

The laser systems based on the sensitized emission can be particularly important for construction of lamp pumped high energy Q-switched or ultra-short lasers based on the Yb^{3+} emission for applications in fundamental physics or inertial nuclear fusion research. Besides the spectroscopic properties of laser materials, large-size laser components, with high thermal conductivity and thermo mechanical parameters would be necessary for such applications. The cubic oxide materials, such as the sesquioxides Ln_2O_3 (Ln = Y, Lu, Sc) or garnets ($Y_3Al_5O_{12}$ – YAG) have high thermal conduction and thermal stress parameter; unfortunately, the size and in many instances the doping concentration and uniformity of the single crystals are limited. The transparent polycrystalline materials produced by ceramic techniques could circumvent many of these difficulties. Yb-doped sesquioxides (Y_2O_3) or garnets (YAG) ceramics have been investigated intensively in recent years for high energy laser emission at room and cryogenic temperatures.

A main condition for efficient sensitization is the overlap of the donor emission with the acceptor absorption. The Cr^{3+} ions in crystals have strong and broad absorption bands in visible, whereas the emission properties are strongly influenced by the strength of the crystal field interaction: in weak fields the energy level $^4T_2$ lies below the level ^2E and gives strong and broad emission in near infrared, whereas in strong crystal fields the relative positions of these two levels is reversed and Cr^{3+} gives sharp red emission [1]. Cr^{3+} ions have been used as sensitizers of several RE^{3+} ions with absorption in red or near infrared, such as Nd^{3+}, Tm^{3+}, Er^{3+}, especially in garnets [1, 3, 4]. The advantage of garnets is the existence of three crystalline sites (dodecahedral, octahedral and tetrahedral) making possible the doping with ions of different dimensions – (Cr^{3+} enters in the small octahedral sites occupied normally by Al^{3+}, Ga^{3+} or Sc^{3+} ions , while RE^{3+} ions enter in the larger dodecahedral sites. In case of the substitution of Al^{3+} or Ga^{3+} the crystal field acting on Cr^{3+} is strong, whereas in the garnets with Sc^{3+} it is weak and the Cr^{3+} emission could be used for very efficient sensitization of Nd^{3+}.

Recently special attention was focused on (Cr, Nd) garnet ceramics to enhance the absorption efficiency in u.v. – visible for solar-pumped lasers [5].

Up to now there are no published data concerning the sensitization by Cr^{3+} ions of Yb^{3+} emission, mainly since there are very few Cr^{3+} doped materials emitting in the range of Yb^{3+} absorption (850-1080nm), that could grant efficient resonant energy transfer to this ion. The sensitization of Yb^{3+} emission with Cr^{3+} ions in garnets is impossible since the crystal field of the octahedral site is too large to grant Cr^{3+} emission in the range of Yb^{3+} absorption, even when Cr^{3+} substitutes Sc^{3+}. This would impose the search for laser materials with weaker crystal field interaction, i.e. with larger substitution sites. In principle, the cubic sesquioxides offer such sites, but the doping with Cr^{3+} of sesquioxides ions is difficult, due to its small ionic radius (0.615 Å in six-fold coordination) compared to Ln^{3+} (Y^{3+} 0.9 Å, Lu 0.86 Å, Sc – 0.745 Å) and has been studied by optical spectroscopy only in Sc_2O_3 single crystals [6, 7]. The high melting temperature of Sc_2O_3 (~ 2420^oC) makes the crystal growth from the melt very difficult and expensive. Besides, the low segregation coefficient of Cr^{3+} connected to the differences in the ionic radii of Cr^{3+} and Sc^{3+}, the evaporation of Cr_2O_3 during growth limits the dopant content. Ceramic techniques could overcome a series of such problems and allow the preparation of larger components, with higher concentrations at lower cost. Preliminary results on Cr^{3+} in Sc_2O_3 ceramics have been reported by our group [8] and they indicate that the emission of Cr^{3+} in infrared encompasses the absorption of Yb^{3+}. The first data on the Yb^{3+} sensitized emission of Cr^{3+} Sc_2O_3: (Cr, Yb) ceramic shall be presented in this paper.

Other ways of sensitization of Yb^{3+} emission have been considered, one of them being by Nd^{3+} ions. The systems based on Nd→Yb energy transfer are interesting since they combine the Yb^{3+} ion good laser emission characteristics with the Nd^{3+} multiple and intense absorption bands that could be used for pumping with different sources (laser diodes, flash lamps, solar radiation, etc). Energy transfer efficiencies over 95% were reported in sesquioxide ceramics (Nd, Yb): Sc_2O_3 [9], or (Nd, Yb): Y_2O_3 [10,11] for rather low Yb^{3+} concentrations; these efficiencies are considerably larger than reported for other materials (see references in [12]). (Nd, Yb): sesquioxide ceramics are considered as potential materials for high power petawatt lasers [13]. Yb^{3+} laser emission in (Yb, Nd): YAG-buried channel waveguide laser pumped at 0.81 μm has been obtained [14] and Nd→Yb energy transfer in GGG single crystals, with efficiency of ~ 84% for ~ 6 at.% Yb has been reported recently [15].

The aim of this paper is to investigate new systems for the sensitization of Yb^{3+} emission, mainly co-doped oxide transparent ceramics, the accent shall be on (Nd, Yb): YAG and (Cr, Yb): Sc_2O_3.

2. EXPERIMENTAL DETAILS

The transparent ceramic samples of YAG single doped with Yb (1-5 at. %) or Nd (1-2 at. %) and two series of co-doped samples with variable Yb content (Ybx, x = 1, 3, 5 at. %) and fixed Nd content at 1 and 2 at. %, (denoted by NdyYbx), were prepared by solid state synthesis that involve oxides mixing, isostatic compressing and sintering at ~ 1750^0C [16]. These ceramics have grains of tens of microns, nm grain boundaries and low density of inter-grain pores (~ 1 ppm in volume). Both ions enter in Y^{3+} dodecahedral sites, of D_2 local symmetry in the cubic Ia3c space group of YAG.

Samples of Sc_2O_3 single doped with Cr^{3+} Sc_2O_3 (0.1, 0.2 at. %) and (Cr, Yb) co-doped with 0.2at. % Cr and Yb 1 and 3 at. % were obtained by solid state synthesis [17]. In the cubic group Ia3 lattice of Sc_2O_3, the Sc^{3+} ions occupy two sites with six-fold oxygen coordination and two vacancies: an axially distorted octahedral site of C_{3i} symmetry (two vacancies on a body diagonal) and a site of C_2 symmetry (two vacancies on a face diagonal) in the ratio 1:3.

The spectroscopic static measurements involve high-resolution absorption and emission at different temperatures from 10-300K. An experimental set-up containing: a tungsten halogen lamp, one-meter Jarell Ash monochromator, and a Lock – in SRS amplifier connected to a computer, a closed cycle He refrigerator ARS-2HW was used. The emission was excited with a lamp, or laser diodes at 670 nm, 970 nm. The emission kinetics were measured by laser excitation with 532 nm – the second harmonic of a YAG: Nd Quanta Ray (~ 10 ns) and a multichannel scaler MCS-PCI ORTEC.

3. THEORETICAL CONSIDERATIONS ON THE SENSITIZATION PROCESSES

The sensitized emission implies an energy transfer from a donor D to an acceptor A and can be evidenced by analyzing the experimental donor and acceptor emission spectra and decays when only the donor is excited, function on different factors (time, doping concentrations, temperature, etc.).

In presence of energy transfer the temporal evolution of the normalized emission of the donor D, after a short excitation pulse, could be written as

$$I_D(t)/I_0 = \exp\left[-\frac{t}{\tau_{0D}} - P_{D-D}(t) - P_{D-A}(t)\right], \quad (1)$$

where τ_{0D} is the D isolated ions lifetime, $P_{D-D}(t)$ transfer function describes the non-exponentiality due to energy transfer inside donor system (cross relaxation,

etc) and $P_{D-A}(t)$ is the transfer function related to D→A transfer. Both transfer functions could contain a direct type of transfer to acceptors and quenching associated to migration on donors, depending on the system and doping concentrations.

Since we are interested in the D→A energy transfer characteristics, a simple way is to use single doped and co doped samples with the same D content. This is possible in ceramics since one could control the concentrations of the sample, the actual dopants content in the sample is alike to that of the raw material. This way one could extract from experimental data $I_D(t)/I_0$ the P_{D-A} transfer function and then follow its dependence on time, D and A concentrations, temperature, etc. in order to determine the energy transfer mechanisms and parameters. If the direct D–A transfer is large, comparatively to migration on donors, the transfer function $P_{D-A}(t)$ for a random distribution of the acceptors around the donor could be written as [18]

$$P_{D-A}(t) = \sum_i \ln\left[1 - C_A + C_A \exp(-W_{DA}^i t)\right], \tag{2}$$

where C_A is the relative acceptors concentration, W_{DA}^i is the transfer rate to the acceptor placed at site i with respect to donor and the summation is performed on the sites i available to acceptors. For multipolar interactions $W_{DA}^i = \frac{C_{DA}^{(s)}}{R_i^s}$, with R_i – the distance to acceptor i, $C_{DA}^{(s)}$ – the transfer microparameter and s is the multipolarity (with s = 6 for dipole-dipole, s = 8 for dipole-quadrupole and s = 10 for quadrupole-quadrupole). The energy transfer microparameters $C_{DA}^{(s)}$ are determined by the spectral characteristics (electronic structure, absorption and emission cross sections, etc) of the D and A ions, particularly by the superposition of the donor emission and acceptor absorption for the transitions involved in transfer.

At the beginning of the decay, when the products $W_{DA}^i t$ in (2) are small, the transfer function could be approximated with a linear function on t, while at longer times, the sum can be replaced by an integral, and for multipolar interactions one have

$$P_{D-A}(t) = W_{st} t \quad \text{for } t < t_1, \qquad \text{and} \qquad P_{D-A}(t) = \gamma^{(s)} t^{3/s} \quad \text{for } t > t_1, \tag{3}$$

where W_{st}, the slope in origin and $W_{st} = \sum_i C_{DA} C_A$. Both parameters, W_{st} and $\gamma^{(s)}$ [19] depend linearly on acceptors concentration C_A, for dipole–dipole interaction one have

$$\gamma = \frac{4}{3}\pi^{3/2} n_A (C_{DA})^{1/2} t^{1/2}, \tag{4}$$

where n_A is the absolute concentration of acceptors, where for simplicity the index $s = 6$ was dropped. The time border t_1 between the two time regimes is diffuse and depends on the transfer mechanisms in the particular system as shall be discussed later in the concrete cases. The energy transfer microparameters can be thus inferred from the shape and dependence of the emission decay on the acceptor concentration.

The emission quantum efficiency in presence of transfer is

$$\eta_{qe} = \frac{1}{\tau_D} \int \frac{I_D(t)}{I_0} \mathrm{d}t \tag{5}$$

and can be used for the definition of an effective lifetime of the donor in presence of transfer, $\tau_{D-A} = \tau_D \eta_{qe}$. The emission quantum efficiency and τ_{D-A} can be calculated with equation (5) and the measured energy transfer parameters or it can be simply estimated from the area under the normalized decay curves and the energy transfer efficiency can be evaluated from

$$\eta_{tr} = 1 - \eta_{qe} = 1 - \frac{\tau_{D-A}}{\tau_D}, \tag{6}$$

4. SPECTRAL DATA

4.1. Nd →Yb energy transfer in YAG

According to the discussion of the Section 3, the efficiency of the Nd→Yb energy transfer is determined by the energy transfer microparameters and by the absolute doping concentrations. The evaluation of a sensitized system requires accurate spectral data on single doped and co-doped material. The spectral data of Nd^{3+} or Yb^{3+} in YAG ceramics have been intensively analyzed, observing similarities and differences from single crystals (higher content of RE ions aggregates -pairs, triads-, lower non-stoichiometric effects, etc.) [20–24]. From the analysis of the Stark structure of both ions it is clear that a resonant Nd → Yb energy transfer, involving Nd^{3+} $^4F_{3/2} \rightarrow {}^4I_{9/2}$ emission and Yb^{3+} $^2F_{7/2} \rightarrow {}^2F_{5/2}$ absorption is possible in YAG, according to the scheme presented in Fig. 1.

The Nd→Yb energy transfer microparameters are proportional to the super position of the Nd^{3+} emission with the Yb^{3+} absorption as shown with 300 K data in Fig. 2; Nd^{3+} emission cross sections were estimated with the reciprocity method. The overlap depends on the position and Stark structure of the manifolds involved in the transfer and the cross-sections of the corresponding transitions.

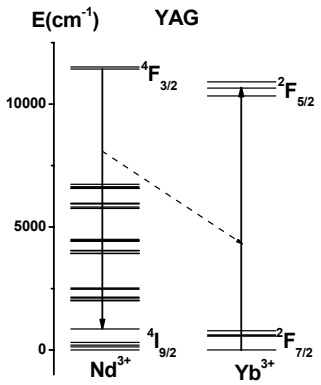

Fig. 1 – The Stark Nd^{3+} and Yb^{3+} levels in YAG and schematic Nd→Yb energy transfer.

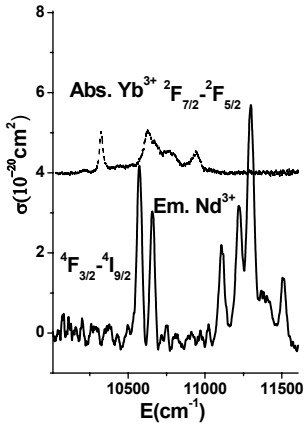

Fig. 2 – Nd^{3+} emission and Yb^{3+} absorption cross sections in YAG at 300 K.

The data from Fig. 2 show clearly that the Yb^{3+} absorption lines involved in the transfer correspond to the electronic transition $^2F_{7/2}$ (1) → $^2F_{5/2}$(2) and nearby vibronics [24], and the main Nd^{3+} emission lines are $^4F_{3/2}$ (1,2) → $^4I_{9/2}$ (5), where the numbers in parentheses indicate the Stark levels of the manifolds. Thus, by exciting Nd^{3+} in various spectral ranges (with different sources), the metastable Nd^{3+} level $^4F_{3/2}$ is populated and can transfer its excitation to Yb^{3+} ions by non-radiative resonant energy transfer.

The presence of the Nd→Yb energy transfer can be confirmed by following the Yb^{3+} emission when exciting Nd^{3+} with a filtered lamp in visible absorption bands as shown in Fig. 3 for Nd1Ybx (x = 1, 3, 5 at. %) samples: the ratio of Yb^{3+} emission to the residual Nd^{3+} emission increases linearly with Yb^{3+} content – in this concentration range (insert of Fig. 3). At low temperatures the energy transfer is less efficient due to the depopulation of the second Stark level $^4F_{3/2}$ (2) of Nd^{3+} and weakening of the vibronic satellites in the Yb^{3+} absorption. The data suggest only a negligible resonant Yb → Nd in YAG back transfer at 300 K, due to low population of $^4I_{9/2}$ (5) Nd^{3+} and $^2F_{5/2}$ (2) Yb^{3+} levels; at 80 K it is entirely eliminated.

The Nd → Yb energy transfer was also demonstrated by measuring the Nd^{3+} $^4F_{3/2}$ or Yb^{3+} $^2F_{5/2}$ emission decays in the (Nd, Yb) co-doped samples under Nd excitation with a pulsed laser (10 ns) at 532 nm. This energy transfer competes with the selfquenching of Nd^{3+} emission due to the cross-relaxation ($^4F_{3/2}$, $^4I_{9/2}$)→($^4I_{15/2}$, $^4I_{15/2}$) [20–23]. The global Nd → Yb transfer efficiencies were estimated by comparing the Nd^{3+} $^4F_{3/2}$ decay in single doped and (Nd, Yb) co-doped samples with the same Nd^{3+} content and with different Yb^{3+} concentrations by using experimental effective lifetimes τ_{Nd} and τ_{Nd-Yb} (the area under normalized decay curves) and relation (6). The Nd →Yb transfer efficiency increases with

Yb^{3+} content, being of ~ 83% for Nd1Yb5: YAG sample at 300 K, but it could be further increased for larger Yb^{3+} concentrations. For larger Nd^{3+} concentrations, the onset of migration of energy on donors increase both the Nd^{3+} selfquenching and the transfer to Yb^{3+}.

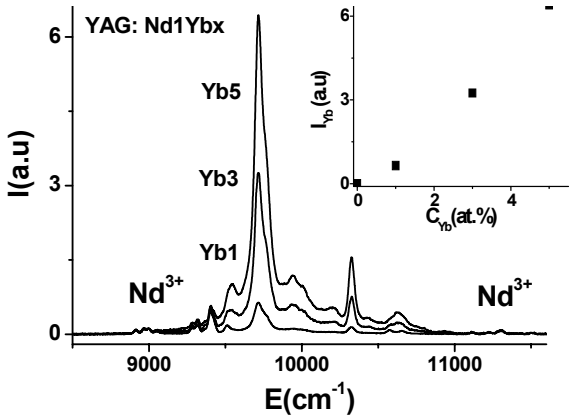

Fig. 3 – I.r. 300K emission of YAG: Nd1Ybx (x = 1, 3, 5) under visible excitation of Nd^{3+}; insert – I_{9700}(Yb) line intensity *versus* Yb^{3+} content.

The Nd→Yb energy transfer mechanisms and parameters were obtained from Nd^{3+} $^4F_{3/2}$ decays in a series of (Nd, Yb):YAG samples with the same Nd^{3+} content, by subtracting the contribution given by Nd →Nd energy transfer at the same Nd^{3+} concentration as described recently [11] in details for Y_2O_3. The analysis of the decay curves indicates that the Nd→Yb energy transfer is dominated by dipole-dipole interaction with the room temperature transfer microparameter $C_{DA}^{\text{Nd-Yb}}$ equal to ~ 2.4×10^{-39}cm^{6}s^{-1}. This parameter is much larger than the Nd →Nd transfer microparameter $C_{DA}^{\text{Nd-Nd}}$ ~ 1.8×10^{-40}cm^{6}s^{-1}.

4.2. The Cr^{3+}→Yb^{3+} energy transfer characteristics in Sc_2O_3 ceramic

Whereas the optical spectra on Yb^{3+} doped Sc_2O_3 single crystals [25, 26] or ceramics [27–29] have been intensively studied, only few data on Cr^{3+} in Sc_2O_3 single crystal fibers [6] and in the crystals grown by Bridgman or Kyropulos method [7] have been published. The Yb^{3+} ions enter in Sc_2O_3 in both sites C_2 and C_{3i}, but the optical spectra are dominated by Yb^{3+} in C_2 sites; the transitions for C_{3i} local symmetry are only magnetic dipole allowed, the lines are less intense, clearly observed in the $^2F_{7/2}$ (1) → $^2F_{5/2}$ (1) range, and difficult to separate in the other transitions due to the interference with strong vibronics.

The optical spectra of Cr^{3+} Sc_2O_3 are complex and have been assigned to Cr^{3+} in octahedral sites (the major center I [6, 7]) and to an unknown center (II) [7] that could be a Cr^{3+} in C_2 site or a Cr ion of a different valence. EPR of weakly Cr^{3+}–doped Sc_2O_3 crystal evidenced only one center of trigonal C_{3i} symmetry [30]; consistent with the preference of Cr^{3+} for octahedral complexes.

Preliminary optical spectroscopic results on Cr^{3+} in Sc_2O_3 ceramics have been reported by our group [11]: the room temperature absorption spectrum of the Cr: Sc_2O_3 ceramics is similar to that reported for single crystals [7] and contains strong unresolved broad bands in UV, and a series of bands in visible and near i.r., peaking at ~ 480 nm and a broad double band peaking at 745 nm and 920 nm.

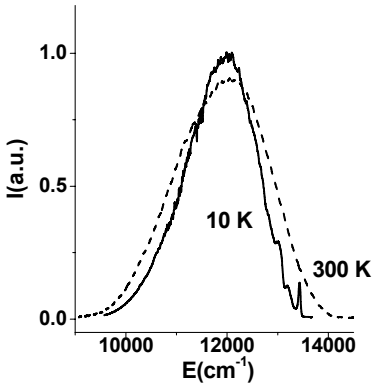

Fig. 4 – Emission spectra of Cr: Sc_2O_3 at 10 K (continuous line) and 300 K (dash line) under 670 nm excitation.

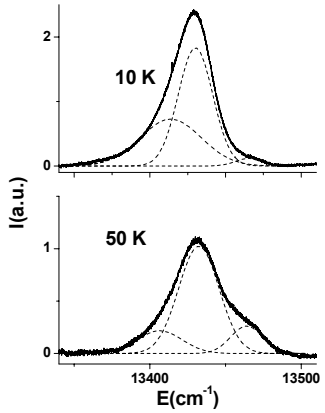

Fig. 5 – Temperature dependence of Cr^{3+} emission in the region of zero-phonon $^4T_2 \rightarrow {}^4A_2$ lines.

The 300 K emission excited with a filtered lamp or ~ 670 nm cw laser diode (at this wavelength, center I is excited) contains a broad band extending between 9,500 and 14,000 cm^{-1} (FWHM ~ 160 nm), with the peak around 870 nm. At low temperatures the emission band narrows (FWHM 115 nm – at 10 K), the peak shifts slightly to lower energies, and sharp lines fine structure (zero-phonon lines) around 744.5 nm (~ 13430 cm^{-1}) (Fig. 4) along with a series of phonon satellites, at ~240, 420, 460 cm^{-1}, are observed.

The emission decay of Cr^{3+} in Sc_2O_3 ceramic at 300 K under 532 nm excitation of center I and detection at ~ 700 nm is non-exponential. For 0.1 at. % Cr^{3+} the decay can be described by a double exponential with lifetimes ~ 20 and 70 μs, similar to data reported in [7]. The nature of this non-exponentiality is not clear, it could be due to Cr-Cr pairs.

Taking into account the preference of Cr^{3+} for octahedral positions and in accord with the previous reports [6,7] one could assign the prevailing center I to Cr^{3+} in the C_{3i} site – a trigonally distorted octahedral symmetry. The lower energy

absorptions of Cr^{3+} in C_{3i} center I in Sc_2O_3 could be assigned to transitions from fundamental level $^4A_2$ to $^4T_2$, ^2E, $^2T_1$, $^2T_2$, $^4T_1$ octahedral levels split by trigonal crystal field and spin-orbit interaction (^2E in two, $^2T_1$, and $^2T_2$ in three and $^4T_2$, $^4T_1$ in four spinor states). The strong absorption spectra in visible at ~ 670 nm and ~ 480 nm could be assigned as previously [7] to transitions from $^4A_2$ to the $^4T_2$, $^4T_1$ cubic split levels of center I. Besides, the dips in the absorption bands (Fano – antiresonances [31]) were tentatively assigned to spin forbidden transitions. Thus, the 711 nm peak could be due to transition to the doublet ^2E, 650 nm and 670 nm peaks to the $^2T_1$ split level.

The fine structure observed in the emission spectra (Fig. 5) could be associated to the zero-phonon lines given by the transitions from the four spinor levels of $^4T_2$ to $^4A_2$. In our spectra we observed three components situated relatively to the lowest one 13410 cm^{-1} at +20 and +55 cm^{-1}. The last two components (separated by ~ 35 cm^{-1}) have been observed previously in Cr: Sc_2O_3 fibers [6], but their relative intensities at 10 and 50 K are different from our data. The intensity of the low energy component decreases at 50 K (Fig. 5), while that of the other two components increase, suggesting that they originate from the thermal zed components of a split excited level ($^4T_2$). Similar fine structure has been detected for Cr^{3+} in ScF_3 [6] or Cr^{3+} spectra in octahedral environment of $LiCaAlF_6$, $LiSrAlF_6$ [32, 33] and have been assigned to spin-orbit splitting of the octahedral term $^4T_2$. Our case is more complicated by the presence of additional trigonal distortion, difficult to evaluate. Such zero-phonon lines have been observed emission [34, 35] and absorption spectra [36] of Ti^{3+} in trigonally distorted Al_2O_3 sites.

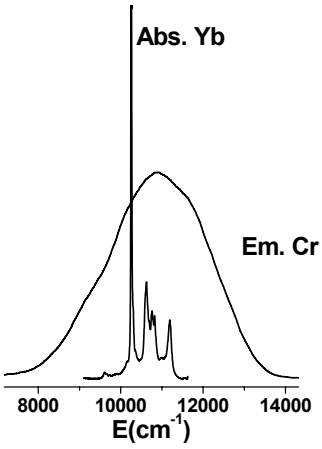

Fig. 6 – The overlap of the Cr^{3+} center I and Yb absorption in Sc_2O_3 ceramic at 300 K.

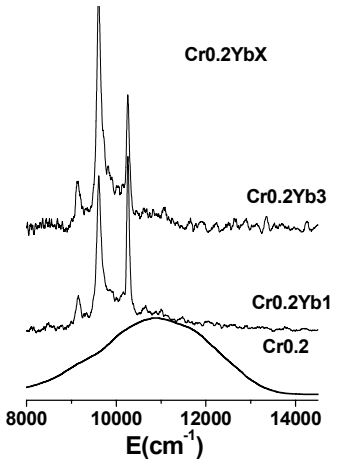

Fig. 7 – The 300 K emission spectra of single doped and Yb co-doped samples under visible 670 nm excitation.

The good overlap (Fig. 6) of $^4T_2 \rightarrow {}^4A_2$ broad emission of center Cr^{3+} I in the 9,000 – 14,000 cm^{-1} range with Yb^{3+} absorption (~ 9,000 – 11,200 cm^{-1}) [25] should assure an efficient resonant energy transfer from Cr^{3+} I to Yb^{3+} in (Cr, Yb): Sc_2O_3 co-doped ceramics. Indeed, efficient Cr → Yb transfer was demonstrated by the emission spectra at 300 K in (Cr, Yb): Sc_2O_3 co-doped ceramic samples under cw 670 nm excitation (Fig. 7) and by the Cr^{3+} emission decays under 532 nm pulsed excitation (Fig. 8). As can be observed in Fig. 7, the Cr^{3+} I center emission is almost quenched in Cr0.2 Ybx (x = 1, 3) co-doped samples, while Yb^{3+} emission increases with Yb^{3+} content; the Yb $^2F_{5/2}(1) \rightarrow {}^2F_{7/2}(1)$ zero-phonon line (at 10255 cm^{-1}) presents re-absorption effects.

The Cr^{3+} emission kinetics at 300 K in the same co-doped (Cr, Yb): Sc_2O_3 samples show clear quenching that increases with Yb^{3+} content (Fig. 8). The Cr→Yb energy transfer efficiency $\eta_{Cr\text{-}Yb}$ can be estimated by using the effective lifetimes of Cr^{3+} emission τ_{Cr} and $\tau_{Cr\text{-}Yb}$ in single doped and (Cr, Yb) co-doped samples with the same Cr^{3+} content and using the relation (6). The transfer efficiency increases with Yb^{3+} content from 60% for Cr0.2Yb1 to 85% in Cr0.2Yb3 sample.

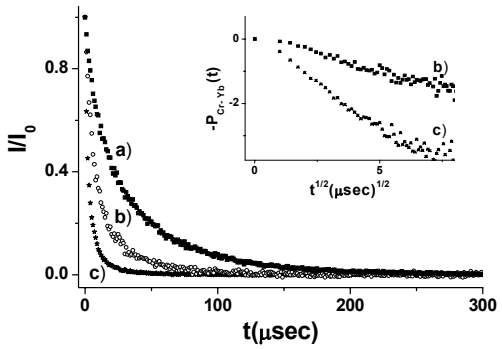

Fig. 8 – The 300 K decays of Cr^{3+} under pulsed 532 nm excitation in: a) Cr0.2; b) Cr0.2Yb1; c) Cr0.2Yb3 samples. Insert, the Cr →Yb energy transfer functions in a $t^{1/2}$ scale.

Though the nature of the non-exponential character of Cr^{3+} emission in Sc_2O_3 is not clarified, one could get some insight into the nature of Cr→Yb energy transfer by analyzing the Cr^{3+} emission kinetics in (Cr, Yb) co-doped samples. Thus, for small Cr^{3+} concentrations, when the migration on the donors could be neglected, the non-exponential Cr^{3+} decays of co-doped samples are due to two direct types of energy transfers Cr→Cr and Cr →Yb as in relation (1); with two terms describing the decay of the single doped Cr^{3+} sample, and one $P_{Cr\text{-}Yb}$, the transfer function corresponding to Cr → Yb energy transfer. In the insert of Fig. 8 the $P_{Cr\text{-}Yb}$ transfer functions, obtained by substracting from the decay curves of

Cr^{3+} in (Cr, Yb) co-doped samples the decay of the single doped samples with the same Cr^{3+} content are presented in a $t^{1/2}$ scale. The $P_{\text{Cr-Yb}}(t)$ curves show two clear time regimes described by equation (3): a linear dependence on t at the very beginning, that evolves gradually into $t^{1/2}$ dependence for $t > 5$ μs, the slopes of both linear and non-linear parts being proportional with Yb^{3+} content. The presence of the two "regimes" has a simple physical interpretation, being the linear (small $W_i t$) and continuous limits of the equation (2). From the long time part of the $P_{\text{Cr-Yb}}(t)$ (Fig. 8), that corresponds to a direct Cr→Yb energy transfer governed by the dipole-dipole interaction, and using the slopes γ in expression (4) and n_A – the absolute concentration of Yb (in both sites), a transfer microparameter $C_{DA}^{\text{Cr-Yb}} \sim 6.4\times10^{-39}\text{cm}^6\text{s}^{-1}$ was estimated.

A rough estimate of t_1, the time border between the two static regimes, is $t_1 \sim \frac{R_{\min}^6}{C_{DA}^{\text{Cr-Yb}}}$ with $R_{\min}$ the shortest donor-acceptor distance. Using the $C_{DA}^{\text{Cr-Yb}}$ microparameter and the distances in Sc_2O_3 from a given C_{3i} site to the near neighbor sites (6 C_2 at 3.24 Å, 6 C_2 at 3.73 Å, 6 C_{3i} at 4.9 Å, 12 C_2 at 5.89 Å, etc.) one could obtain approximate values of t_1. Thus, it is ~ 0.18 μs for the nearest C_{3i}-C_2 neighbors at 3.24 Å, but has a value of ~ 6.5 μs, close to our experimental data, only for C_{3i} -C_2 neighbors at 5.99 Å. A similar behavior has been encountered for Nd : YAG [20-23], and was explained by the presence of a strong short-range interaction – exchange – between Nd ions in the nearest neighbor pairs that determines a fast energy transfer, manifested by a fast drop, within 1-2 microseconds at the beginning of the decay. As discussed in ref. [37], the duration of this drop is determined by the strength of the short-range interaction. In case of the Cr-Yb pairs, a much stronger exchange interaction could be expected, involving more pairs and determining a faster drop at the beginning of decay. The consistency of the value of t_1 in case of the (Cr, Yb): Sc_2O_3 ceramics with the third-order Cr-Yb pair indicates that the first two nearest pairs (separation of 3.24 and 3.73 Å) could be involved in the fast transfer, similar to the case of (Cr, Nd);GSGG [4]; unfortunately, the limited resolution of our equipment (0.1 μs) did not enable observation of such drop at the beginning of decay.

5. DISCUSSION AND CONCLUSIONS

The sensization processes of Yb^{3+} emission are investigated in the attempt to explore the possibilities of pumping the Yb lasers with strong pulsed sources (flash lamps) in visible and obtain high power lasers, with applications in fundamental physics or inertial nuclear fusion research. The materials appropriate for such applications are limited: the good thermo-mechanical properties of the high temperature cubic oxides (sesquioxides or garnets). The possibility to produce

large volumes of highly transparent ceramics with tailored characteristics (composition, doping level and distribution) makes these materials of prospect for high power laser emission. Our attention was concentrated on sensitization of Yb^{3+} emission by Nd^{3+} ions YAG and by Cr^{3+} in Sc_2O_3 ceramics, not investigated previously.

The presence of rather efficient Nd→Yb energy transfer in YAG was demonstrated by the emission of (Nd, Yb) co-doped samples under Nd^{3+} cw visible excitation or by the analysis of the Nd $^4F_{3/2}$ emission decays 532 nm pulsed excitation. The transfer efficiencies, energy transfer mechanisms and parameters were inferred from the analysis of experimental data in terms of the energy transfer theories. It is interesting to compare the sensitization characteristics of Yb^{3+} emission by Nd^{3+} in YAG with those reported recently on (Nd, Yb): Y_2O_3 ceramic [10,11]. For both materials the transfer efficiency increases with Yb^{3+} content in absolute values. Up to 5 at. % the Nd →Yb transfer efficiency increases linearly with Yb content, attaining at 300 K ~ 83% for Nd1Yb5: YAG sample (6.9×10^{20} Yb ions/cm^3), but it could be increased at larger Yb^{3+} content. In the case of the Y_2O_3 ceramic the transfer efficiency has the tendency of saturation, it is ~93% for 3 at.% Yb (8.1×10^{20} Yb ions/cm^3) and ~ 98% for 5 at. % Yb (13.5×10^{20} Yb ions/cm^3). In both cases the Nd→Yb energy transfer is dominated by dipole-dipole interaction with large room temperature transfer microparameters C_{DA}: ~ $2.4\times10^{-39}$$cm^6s^{-1}$ in YAG and much larger, ~ 1×10^{-38} cm^6s^{-1}, in Y_2O_3. These data could be explained by the Stark structure and the overlap integral of Nd^{3+} emission with Yb^{3+} absorption; in YAG the main Nd^{3+} emission lines are $^4F_{3/2}(1,2) \rightarrow {}^4I_{9/2}$ (5), whereas in the case of Y_2O_3 six lines $^4F_{3/2}$ (1,2) → $^4I_{9/2}$ (3,4,5) are involved in the transfer [11]. Therefore, efficient energy transfer from Nd^{3+} to Yb^{3+} at the room temperature can be obtained by a proper selection of the doping concentrations in the Y_2O_3 and YAG ceramics. The lowering of temperature reduces the transfer efficiency and higher Yb^{3+} concentrations must be used to assure large efficiencies. However, as known, the Yb^{3+} laser efficiency and the power scaling potential in cryogenic conditions in YAG [38] or Y_2O_3 [39] increases due to reduction of reabsorption and to the increase of heat conductibility [40]. The spectral data on (Nd, Yb) co-doped YAG or Y_2O_3 suggest the possibility of cryogenic Yb^{3+} sensitized emission in both cases.

The efficient sensitization with Cr^{3+} of Yb^{3+} emission requires materials in which the Cr^{3+} emission overlaps with Yb^{3+} absorption. This could be possible only in laser materials where the $^4T_2$ Cr^{3+} level is lower in energy than the level ^2E; in such case the emission is concentrated in the broad vibronic band of the spin-allowed $^4T_2 \rightarrow {}^4A_2$ transition and extension to infrared of this band would require large substitution sites for Cr^{3+}, such as in case of Scandium laser materials. For this reason the spectral investigation of the single doped Cr: Sc_2O_3 ceramic is important: it revealed the presence of two Cr centers (I, II), as those reported in single crystals [6, 7], both with broad emissions. The prevailing Cr^{3+} center I with the peak at ~ 870 nm, assigned to Cr^{3+} in a C_{3i} site – a trigonally distorted

octahedral symmetry has a good overlap with Yb^{3+} in Sc_2O_3 as illustrated in Fig. 6 for 300 K, the overlap is slightly smaller at low temperatures.

Earlier analysis of the electronic structure (Racah parameters and crystal field splitting) of Cr^{3+} in Sc_3O_3 crystals was based on the positions of the energy levels determined from the maxima of the broad bands in the 300 K absorption spectra. The crystal field parameters determined assuming cubic octahedral symmetry for the C_{3i} center were $Dq \sim 1500$ cm^{-1}, $B \sim 600$ cm^{-1}, $C \sim 3250$ cm^{-1}, $Dq/B \sim 2.5$, i.e. close to the crossing point $^4T_2 \Leftrightarrow {}^2E$ in the Tanabe-Sugano diagram [41], but with ^2E as the lowest level [7]. Although in such case the two excited level would be thermalised, quite strong sharp emission from the level ^2E would be expected together with the thermalised emission form $^4T_2$.

However, the positions of the energy levels in the Tanabe-Sugano diagram, determined from the static interactions inside the doping ion and with the crystal field would correspond normally to the zero-phonon lines in the optical spectra. Based on our room- and low temperature absorption and emission data and on the lack of a strong sharp emission that could be attributed to ^2E emission at low temperatures, an alternative electronic structure can be considered. If the ^2E level position is associated to the Fano anti-resonance observed in the absorption spectra at ~ 14,060 cm^{-1}, and $^4T_2$ is obtained from the zero-phonon line structure at ~ 13,410 cm^{-1}, the $^4T_2$ level for Cr^{3+} C_{3i} center I is slightly lower (~ 650 cm^{-1}) in energy than the ^2E level. This conclusion is consistent with the broad emission of Cr^{3+} center I at 10 K too (Fig. 4), with its lifetime (tens of microseconds) and fairly high emission cross-section.

The spectral (emission and decays) data of (Cr, Yb): Sc_2O_3 co-doped samples show that Yb^{3+} emission can be sensitized with Cr^{3+} in Sc_2O_3 ceramic, with transfer efficiency increasing with Yb^{3+} content from 60% for Cr0.2Yb1 to 85% in Cr0.2Yb3 sample. The analysis of the temporal and Yb concentration dependence of the Cr→Yb transfer function $P_{\text{Cr-Yb}}(t)$ (Fig. 8) revealed the presence of two types of interactions between Cr^{3+} in C_i sites and Yb^{3+}. The decay data could be accurately described if one assumes that the Cr^{3+} and Yb^{3+} near neighbors under 4 Å ($6C_2$ at 3.24 Å and $6C_2$ at 3.73 Å) are coupled by a strong short range interaction, while for larger distances the interaction is of dipolar type with a transfer microparameter $C_{DA}^{\text{Cr-Yb}} \sim 6.4\times10^{-39}$cm^{6}s^{-1}. The quite high energy transfer efficiency from Cr^{3+} to Yb^{3+} in the Sc_2O_3 ceramics indicates the potential of this system for efficient Yb^{3+} emission under visible flash lamp pumping.

Acknowledgements. The present research was was supported by Romanian National Agency for Scientific Research and Innovation, project IDEI- ID- 1240, 503/2009.

REFERENCES

1. A. A. Kaminskii, *Crystaline Lasers*, CRC Press, 1996.
2. D. L. Dexter, J. Chem. Phys. **21**, 836 (1953).
3. E. V. Zharikov, N. N. Il'ichev, V. V. Laptev, A. A. Malyutin, V. G. Ostroumov, P. P. Pashinin, A. S. Pimenov, V. A. Smirnov, and I. A. Shcherbakov, Sov. J. Quantum Electron. **13**, 82 (1983).

4. V. G. Ostroumov, Yu. S. Privis, V. A. Smirnov, and I. A. Shcherbakov**,** J. Opt. Soc. Am. B**, 3**, 81 (1986).
5. T. Saiki, S. Motokoshi, K. Imasaki, K. Yoshida, H. Fujita, and M. Nakatsuga, Opt. Comm., **282**, 1358, 2556 (2009); Jap. J. Appl. Phys, **48**, 122501 (2009).
6.G. Huber, S. A. Payne, L. L. Chase, W.F. Krupke, J. Luminesc, **39**, 259 (1988).
7. S. Kuck, L. Forsaniero, E. Mix, G. Huber, J. Luminesc., **87**, 1122 (2000).
8. V. Lupei, A. Lupei, A. Ikesue, S. Florea, CLEO_EUROPE_EQEC, Paper. CA.P.17 TUE (2009)
9. V. Lupei, A. Lupei, and A. Ikesue, Appl. Phys. Lett., **86**, 111118 (2005).
10. V. Lupei, A. Lupei, C. Gheorghe, S. Hau and A. Ikesue, Optics Letters, **34**, 2141 (2009).
11. V. Lupei, A. Lupei, A. Ikesue, C. Gheorghe, and S. Hau, J. Opt. Soc. Am. B, **27**, 1002 (2010).
12. U. Caldiño, D. Jaque, E. Martín-Rodríguez, M. O. Ramírez, J. García Solé, A. Speghini, and M. Bettinelli, Phys. Rev. B, **77**, 075121 (2008).
13. E. A. Khazanov, and A. M. Sergeev , Physics-Uspekhi **51**, 969 (2008).
14. N. Sugimoto, Y. Ohishi, Y. Katoh, A. Tate, M. Shimokozono and S. Sudo, Appl. Phys. Lett., **67,** 582 (1995).
15. Z. Jia, A. Arcangeli, X. Tao, J. Zhang, C. Dong, M. Jiang, L. Bonelli, and M. Tonelli, J. Appl. Phys, **105,** 083113 (2009).
16.A. Ikesue, T. Kinoshita, K. Kamata, K. Yoshida, J. Am. Ceram. Soc**.,** **78**, 1033 (1995).
17. A. Ikesue, K. Kamata, and K. Yoshida, J. Am. Ceram. Soc., **79**, 359 (1996).
18. S.I. Golubov and Yu.V. Konobeev, Sov. Phys. Solid State, **13,** 2679 (1972).
19. M. Inokuti and F. Hirayama, J. Chem. Phys., **43**, 1978 – 1989 (1965).
20. V. Lupei, A. Lupei, and A. Ikesue, J. Alloys and Comp**.**, **380**, 61 (2004).
21. V.Lupei, A. Lupei, N. Pavel, T. Taira, and A. Ikesue, Appl. Phys. B., **73,** 757 (2001).
22. V. Lupei, Optical Materials**, 19,** 95 (2001).
23. V. Lupei, A. Lupei, Phys. Rev. B, **61**, 8087 (2000).
24. A. Lupei, V. Lupei, C. Presura, V. N. Enaki, andA. Petraru, J. Phys. Condens. Mat., **11**, 3769 (1999).
25. K. Petermann, G. Huber, L. Forsaniero, S. Kuch, E. Mix, V. Peters, and S. A. Basun, J. Luminesc., **87**, 973 (2000).
26. S. Simura, A. Jouini, M.Ji_Hun, A. Brenier, A. Yoshikawa, G. Boulon, and T. Fukuda, Optical Mat., **30**, 18 (2007)
27. J. Lu, J. F. Bisson, K. Takaichi, T. Uematsu, A. Shirakawa, M. Musha, K.Ueda, H. Yagi, T. Yanagitani, and A. A. Kaminskii, Appl. Phys. Lett., **83**, 1101-1103 (2003).
28. G. Boulon and V. Lupei, J. Luminesc., **125**, 45 (2007).
29. L. D. Merkle , G. A. Newburgh, N. Ter-Gabrielyan, A. Michael, and M. Dubinskii, Opt. Com. **281**, 5855 (2008).
30. H. H. Tippins, Phys. Rev., **158**, 301 (1967).
31. M.D. Sturge, H. J. Guggenheim, and M.H. L. Pryce, Phys. Rev. B, **2**, 2459 (1970).
32. S. A. Payne, L.S. Chase, and G.D. Wilke, J. Luminesc., **44**, 167 (1989).
33. M.N.Sanz –Ortiz, F. Rodrigues, R. Valente, J. Phys. Condens. Matter, **22**, 125502 (2010).
34. B.F. Gachter and J.A. Koningstein, J. Chem. Phys., **60**, 2003 (1974).
35. B. Henderson, R. H. Bartram, *Crystal Field Engineering of Solid State Laser Materials*, Cambridge Univ. Press, 2000.
36. A. Lupei, V. Lupei, C. Ionescu, H. G. Tang, and M. L. Chen, Opt. Comm., **59**, 36 (1986).
37. V. Lupei, A. Lupei, S. Georgescu, and I. Ursu, Appl. Phys. Lett., **59**, 905 (1991).
38. D. J. Ripkin, J. R. Ochoa, R. L. Aggarwal, and T. Y. Fan, Opt. Lett., **29**, 2154 (2004).
39. G. L. Bourdet, O. Casagrande, N. Deguil-Robin, and B. LeGarrec, J. Phys. : Conf. Series, **112**, 032054 (2008.)
40. D. C. Brown, IEEE J. Sel. Top. Quantum Electron., **11**, 517 (2005)
41. S. Sugano, Y. Tanabe, H. Kamimura, *Multiplets of Transitional-Metal Ions in Crystals*, Academic, New York, 1970.